https://doi.org/10.5194/egusphere-2025-2936
Preprint. Discussion started: 3 July 2025

Wave-induced sediment resuspension in the Finnish Archipelago, Baltic Sea: Combining small-scale in situ measurements and large-scale numerical model simulations

Jan-Victor Björkqvist[1], Mari Savela[2,3], Heidi Pettersson[4], Victor Alari[5], and Alf Norkko[3]

[1]Norwegian Meteorological Institute, Allégaten 70, 5007, Bergen, Norway
[2]City of Helsinki, Työpajankatu 8, 00580 Helsinki, Finland
[3]Tvärminne Zoological Station, Faculty of Biological and Environmental Sciences, University of Helsinki, J.A. Palméns väg 260, 10900 Hangö, Finland
[4]Finnish Meteorological Institute, P.O. Box 503, 00101, Helsinki, Finland
[5]Department of Marine Systems, Tallinn University of Technology, Akadeemia tee 15a, 12618 Tallinn, Estonia

Correspondence: Jan-Victor Björkqvist (janvb@met.no)

Abstract.

Sediment resuspension, driven by wind-wave-induced shear stresses, plays a crucial role in coastal water quality, biogeochemical cycles, and the dispersal of pollutants and organisms. If the shear stress from waves exceeds an erosion threshold, or critical shear stress, sediments are resuspended from the seabed. This critical shear stress is an essential parameter in sediment transport models, as it determines sediment erodibility. In this study, we implemented a high-resolution (20 m) spectral wave model to simulate wave-induced near-bottom velocities across the complex archipelago of southwestern Finland. Near-bottom shear stresses from the model and their respective critical values were estimated using seabed data, with results compared to critical shear stress values obtained through laboratory testing of in situ sediment samples. Model data suggested that the critical shear stress could be exceeded over 70 % of the time in certain areas. However, laboratory-determined critical shear stresses were 3–8 times higher than those derived from the model based on median grain size, with modelled shear stresses rarely exceeding the measured critical values. These discrepancies likely stem from unaccounted-for biological and biogeochemical properties of the sediments, which cannot be captured by a simple grain size-based model. We estimate that the accuracy of the wave model data used in this study are of secondary importance compared to the uncertainty of determining the critical shear stress.

1 Introduction

Sediment resuspension plays a key role in shallow coastal environments by influencing water quality, nutrient dynamics, and overall ecosystem health. It can release contaminants and nutrients from the sediment, increase turbidity, and redistribute sed-

https://doi.org/10.5194/egusphere-2025-2936
Preprint. Discussion started: 3 July 2025

iment particles, thereby affecting biogeochemical cycles and primary production, altering seabed morphology, and modifying benthic habitat structures.

Sediment resuspension dynamics in coastal areas are primarily governed by wind waves and currents, which exert a shear stress τ ($\mathrm{N\ m^{-2}}$) on the sediment surface. In shallow areas, wave motion is especially influential, as it exerts greater stress on the seabed compared to unidirectional flow, even when instantaneous velocities are similar (Komar and Miller, 1973). Shear stress on the sediment surface mobilizes sediment by dragging and lifting particles, while the gravitational and frictional forces within the sediment resist erosion (Shields, 1936; Soulsby and Whitehouse, 1997). When shear stress exceeds the critical shear stress (τ_{cr}), particle motion initiates, lifting sediment from the seabed into the water column; this process is known as resuspension.

The critical shear stress, which determines the potential for sediment resuspension, is influenced by the sediment's physical and biogeochemical properties (Grabowski et al., 2011). Among these, sediment grain size is one of the most fundamental characteristics, as it largely regulates sediment erodibility. Other key properties include e.g. bulk density, water content, clay mineralogy, and organic content. In sandy sediments, critical shear stress is primarily governed by grain size, whereas in finer, muddy sediments, cohesive forces – caused by electrochemical and biological interactions – become increasingly significant (Black et al., 2002; Roberts et al., 1998).

In addition to physical and geochemical properties, benthic fauna can substantially modify the sedimentary environment through bioturbation, feeding activities, and by altering porosity (Mulsow et al., 1998; Michaud et al., 2006; Harris et al., 2015). The influence of macrofauna on sediment stability depends on the organism's size, abundance, morphology, and functioning in and on the sediment (Grabowski et al., 2011; Harris et al., 2015). Furthermore, vegetation dampens hydrodynamic forces acting on the seabed and stabilizes sediments by binding sediment particles with roots and rhizomes (Koch et al., 2006; Madsen et al., 2001). As a result, critical shear stress and resuspension potential can vary considerably in time (Joensuu et al., 2020) and space (Joensuu et al., 2018).

The critical shear stress is also a key parameter in sediment transport models, where it is often estimated based on median grain size d_{50} (m), as illustrated in Hjulström and Postma diagrams (Dade et al., 1992; Grabowski et al., 2011). However, in natural sediments, critical shear stress can vary significantly, increasing up to fourfold in spring and summer due to seasonal dynamics (Le Hir et al., 2007). For example, the succession of microphytobenthos can stabilize sediment surfaces through biofilm formation during spring blooms (Decho, 2000).

Our aim in this study is to improve understanding of the discrepancies between modelled and observed sediment erosion and resuspension. Bridging this gap is essential for advancing knowledge of coastal dynamics and ecosystem processes, and the physical and biological forces that influence them. In this study, we compare modelled shear stresses with in situ measurements — an approach that remains uncommon in sediment transport research, where empirical data are often limited or absent.

To accurately predict sediment erosion and resuspension in coastal areas, we need an estimate of the magnitude and variation of the near-bottom shear stress and its critical threshold values. The objectives of this study are *i)* to use high-resolution wave simulation to map the spatial variability of the near-bottom shear stresses, *ii)* to use the best available spatial seabed model data

https://doi.org/10.5194/egusphere-2025-2936
Preprint. Discussion started: 3 July 2025

in combination with in situ samples to estimate median grain size and evaluate corresponding critical shear stresses against laboratory measurements, and *iii)* to produce a first estimate of sediment resuspension probabilities based on model data.

Our study area is located in the Hanko archipelago on the northern coast and entrance of the Gulf of Finland, the Baltic Sea (Fig. 1). This region provides an optimal setting for investigating sediment resuspension processes as it is characterized by a mosaic of islands with a diverse range of coastal habitats that capture the spatial variability in seabed composition and encompass the main physical and biological factors regulating sediment erodibility and resuspension dynamics.

The Baltic Sea is a semi-enclosed, brackish, and shallow sea, with a mean depth of 54 m and negligible tidal currents. In the study area, bottom currents are generally weak, ranging from a few centimeters per second to a maximum of 10 $\mathrm{cm\ s^{-1}}$ under typical conditions (Westerlund et al., 2018). However, current speed can exceed 10 $\mathrm{cm\ s^{-1}}$ occasionally in narrow channels or during upwelling events (Westerlund et al., 2018; Miettunen, 2024). Consequently, sediment resuspension in this area is predominantly governed by wind-wave induced shear stresses. The prevailing winds in the area are from southwest, with an average speed of 7–8 $\mathrm{m\ s^{-1}}$ (Alenius et al., 1998).

We simulated the coastal wave conditions using a high-resolution wave model, estimated seabed grain sizes based on publicly available data, and compared our model estimates of median grain sizes and critical stress values with previously gathered field data (Joensuu et al., 2018, 2020). By quantifying differences between modelled and observed erosion thresholds, this study highlights the importance of incorporating empirical data into sediment transport models. A more accurate understanding of sediment erodibility and resuspension dynamics provides valuable insights for the effective management, conservation, and restoration of coastal zones.

This paper is structured as follows: Section 2 describes the measured and modeled data used in this study, Section 3 presents the modeled estimates of shear stress and compares them to observed values, and Section 4 discusses our findings. Section 5 concludes our findings.

2 Materials and Methods

2.1 Measurements

2.1.1 Wave buoy data

Wave observations near Tvärminne were available from two locations in March and April 2017. A larger 90 cm Datawell Directional Waverider Mk-III (Datawell, 2017) was moored at approximately 25 meters depth on the outer edge of the Hanko archipelago (Fig. 2, outer wave buoy). A smaller 40 cm DWR-G4 Directional Waverider was moored north in the archipelago at a depth of roughly 20 meters (Fig. 2, inner wave buoy). Both buoys were located about 3 km east of the Tvärminne research station.

Each wave buoy sampled at a frequency of 1.28 Hz and calculated the wave spectrum up to 0.58 Hz. Low-frequency data (below 0.05 Hz) were discarded when calculating wave parameters.

https://doi.org/10.5194/egusphere-2025-2936
Preprint. Discussion started: 3 July 2025

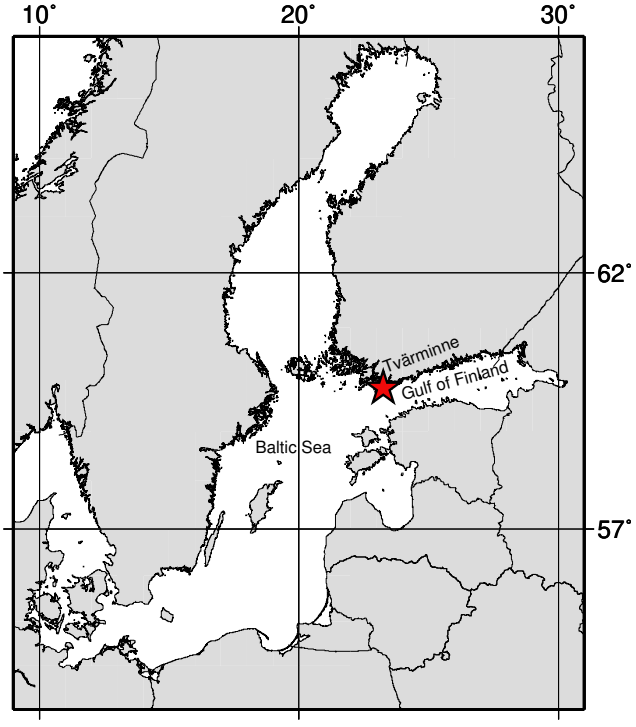

Figure 1. Location of the Tvärminne research station in the western Gulf of Finland, Baltic Sea.

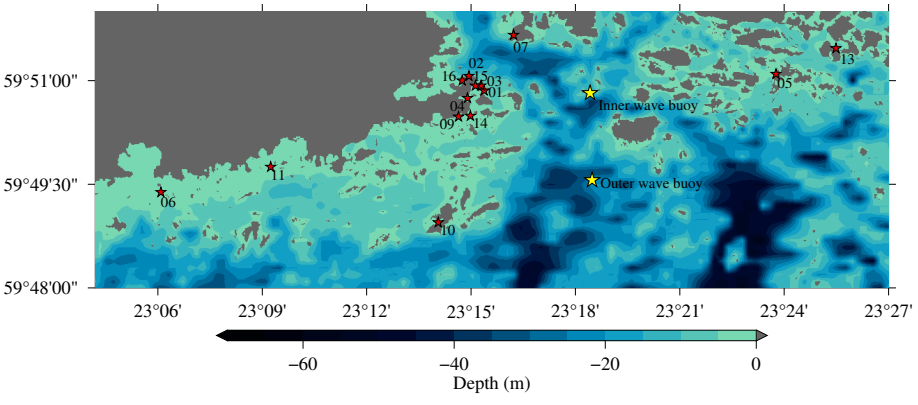

Figure 2. The bottom topography, in situ sediment sampling stations (01–16, marked by red stars), and wave buoy locations (yellow stars) are shown.

2.1.2 In situ sediment samples

Critical shear stress measurements were available from two field campaigns conducted in the years 2014 (Joensuu et al., 2018) and 2015 (Joensuu et al., 2020) in the Hanko archipelago. In 2014, samples were gathered from 16 shallow sites (depth < 4

https://doi.org/10.5194/egusphere-2025-2936
Preprint. Discussion started: 3 July 2025

m), covering a sedimentary gradient from mud to sand (grain sizes 21 μm-570 μm). These sampling locations are illustrated in Fig. 2. The 2014 field campaign focused on spatial variation in sediment erodibility, maximizing variation in sediment surface characteristics (e.g. bedforms, biofilms) across sites. In 2015, three sites (mud (site 4), mixed (site 9), and sandy (site 14) sediment) from the 2014 study were re-sampled from April to December to capture temporal variation in sediment erodibility. In this campaign, variation in sediment characteristics was minimized to focus solely on temporal changes.

The sampling procedure was consistent across both campaigns. At each site, SCUBA divers collected samples by carefully inserting EROMES cores (10 cm diameter, 10 cm depth) into the sediment. Samples were maintained at in situ temperatures and transported to the laboratory for further measurements. A total of 59 and 73 EROMES cores were collected in 2014 and 2015, respectively. For a detailed description of the sampling procedures, see Joensuu et al. (2018) and Joensuu et al. (2020).

2.2 Modelled data

2.2.1 Wave simulations

The SWAN model (Booij et al., 1999) is a spectral wave model that was developed especially for shallow water and nearshore simulations. We implemented SWAN for 1 August – 30 September 2014 to catch the spatially extensive sediment measurement campaign, for 1 May – 30 November 2015 to cover the temporally extensive sediment campaign, and 1 March – 30 April 2017 to cover the period of the wave measurements (for validation purposes). Simulations were forced by data from a numerical FMI-HIRLAM weather prediction system (e.g. Eerola, 2013), where the wind speed and direction had been processed to a height of 10 meters. The wind data had a spatial resolution of roughly 7.4 km, and a 1 h temporal resolution for the years 2014 and 2015, and 3 h for 2017.

The model was implemented to a 0.01 nmi ($\sim$ 20 m) regular grid with lateral boundary conditions taken from a 1 nmi Baltic Sea wide SWAN simulation using the same wind forcing. A 0.01 nmi resolution is higher that what is typically used in wave models, but SWAN has been implemented on a similar resolution before in the Baltic Sea (Alari and Raudsepp, 2012). Another spectral model has also been implemented on the North-American coast with an adaptive resolution up to 10 m (Abdolali et al., 2020) The available bathymetric data had a resolution of 0.1 nmi, but the land–sea mask was available at a 0.01 nmi resolution, and land points were edited to wet points in the 0.1 nmi bathymetrical grid using the surrounding depth information. Additional depth information from Joensuu et al. (2018), Valanko (2012), and field sampling were used. The final 0.1 nmi grid was bi-linearly interpolated to a resolution of 0.01 nmi and the land-sea mask was applied (Fig. 2).

The wave model produced direct hourly gridded estimates of the maximum near-bottom orbital velocity, U_{bot} (m s^{-1}), and the near-bottom mean periods, $T_{m_{bot}}$ (s). The near-bottom amplitudes, a_{bot} (m), were determined directly by the velocity and period estimates. For a full definition of the wave parameters, see Appendix A.

During the simulation periods, the modelled prevailing wave direction at the outer wave buoy was around 225 degrees, and all waves with a height of 2 m or over came from direction between 175 and 225 degrees. The highest significant wave height of 2.9 m was during a wave event from 195 degrees with mean wave periods up to 5.8 s. The simulation period also captured high waves (up to 1.7 m) from the east (95 deg), although these were less frequent. This distribution aligns with the dominant

https://doi.org/10.5194/egusphere-2025-2936
Preprint. Discussion started: 3 July 2025

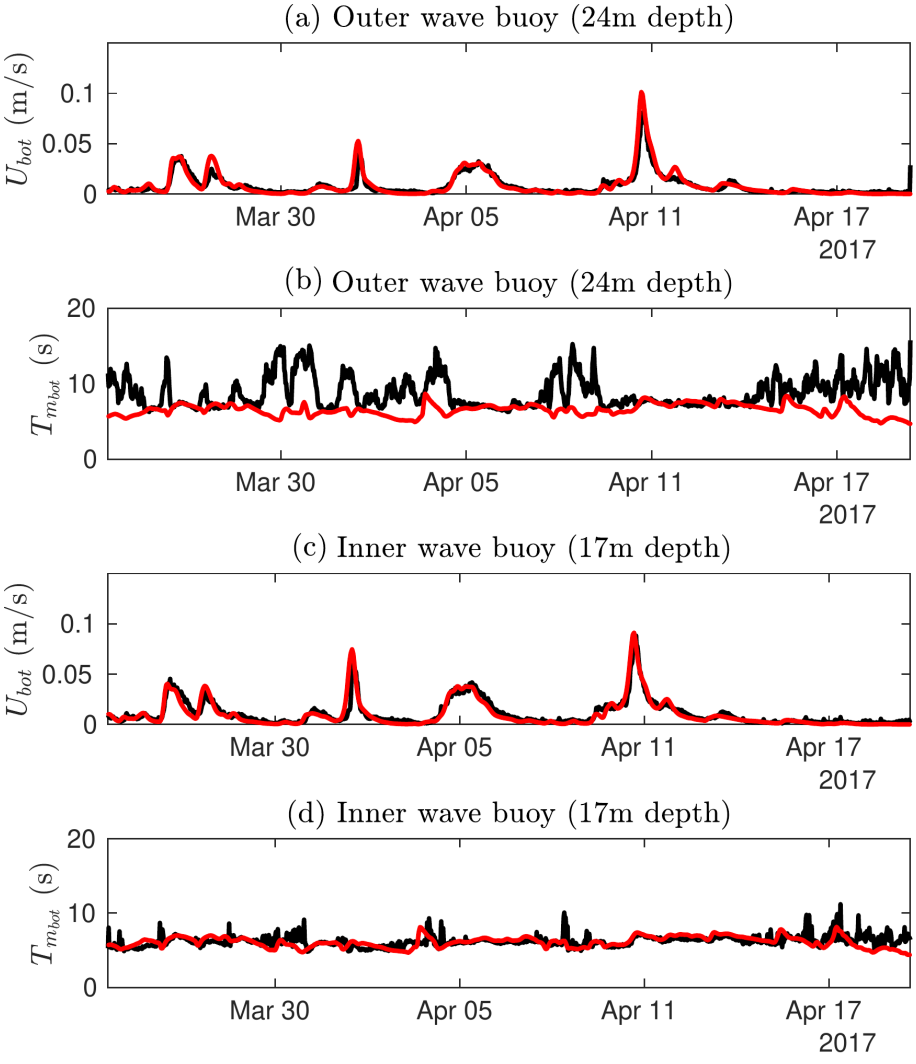

Figure 3. Wave-induced near-bottom orbital velocities and wave period calculated by the SWAN model (red) and the wave spectra measured by wave buoys (black).

directions observed in the Gulf of Finland (Pettersson et al., 2010). Statistics of the modelled near-bottom velocities can be found in Appendix B.

We validated the modelled near-bottom orbital velocities and wave periods by determining them from the measured wave spectrum using the same water depth as in the bathymetrical grid used in SWAN. Near-bottom velocities were modeled accurately at both locations (Fig. 3a&c) with the more exposed outer location showing a -0.04 $\mathrm{cm\ s^{-1}}$ bias and 0.47 $\mathrm{cm\ s^{-1}}$ root-mean-square-error (RMSE). The slightly shallower inner location had a 0.08 $\mathrm{cm\ s^{-1}}$ bias and 0.49 $\mathrm{cm\ s^{-1}}$ RMSE. The modeled near-bottom periods (Fig. 3b&d) were also in good accord with the measurements at the inner location with a 0.12 s

https://doi.org/10.5194/egusphere-2025-2936
Preprint. Discussion started: 3 July 2025

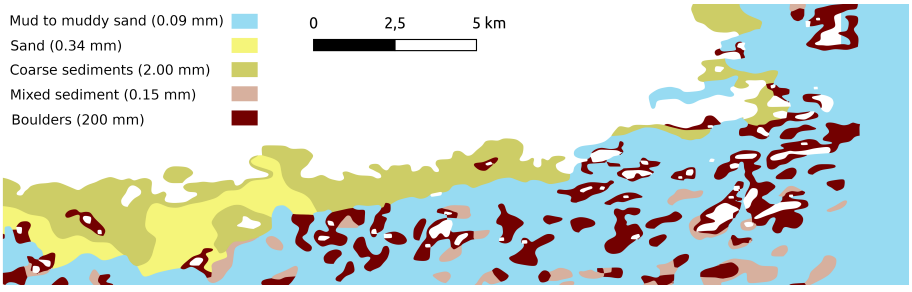

Figure 4. Bottom type classifications from EMODNET data. Corresponding critical shear stresses for representative grain sizes are shown in Table 1.

bias and 0.88 s RMSE. For the deeper location the bias was 2.23 s and RMSE 3.31 s. The clearly worse validation statistics for the outer location is caused by the deeper water depth; the wave orbital motions do not reach the bottom, and the period is determined by low-frequency noise in the measurements. As seen in Fig. 3b, the near bottom periods were modelled well during the higher near bottom velocities, but were less well-defined during very calm conditions. All in all, the modelled wave data is sufficiently accurate for this study's purposes.

2.2.2 Modelled seabed data

No direct observations of the seabed type are available at an extent and resolution that could be combined with the wave model data. We therefore based our calculations on data from EMODNET (Seabed Substrates data 1:100k), where the sea floor type has been classified into five categories: Mud to muddy sand, Sand, Coarse sediments, Mixed sediments, and Boulders (Kaskela et al., 2019). An overview of these classifications for the study area is presented in Fig. 4.

The EMODNET dataset does not give representative median grain size (d_{50}) for the five categories. Representative grain sizes for Mud, Sand, and Mixed sediments were determined from in situ measurements. For Coarse sediments and boulders, we used data from the Geological Survey of Finland, which provides minimum, mean, and maximum grain sizes for each class (Kaskela et al., 2019). We used minimum grain size values as representative d_{50} values, given that the mean sizes are exceptionally large. Since finer grains are the first to be mobilized under increasing shear stress, using the minimum grain size provides a more realistic estimate of the threshold conditions for sediment movement. An overview of the chosen representative grain sizes is provided in Table 1.

2.3 Estimates of seabed shear stress

2.3.1 Modelled shear stresses, τ_w

The shear stress values were modelled based on the near bottom wave induced movements simulated by SWAN, and the estimated grain size (EMODNET).

The shear stress was calculated as:

https://doi.org/10.5194/egusphere-2025-2936
Preprint. Discussion started: 3 July 2025

Table 1. Representative grain sizes and corresponding critical shear stresses for each sediment class.

Sediment class	Grain size (mm)	τ_{cr}(N m^{-2})^a
Mud to muddy sand	0.09	0.14
Sand	0.34	0.21
Coarse sediments	2.00	1.20
Mixed sediments	0.15	0.16
Boulders	200.00	178.10

^{a} Assuming constant values: $\rho_w = 1003$ kg m^{-3}, $\rho_s = 2650$ kg m^{-3}, $\nu = 1.3 \cdot 10^{-6}$ m^2 s^{-1}

$$\tau_w = 0.5 \rho_w f_w U_{bot}^2, \tag{1}$$

where $\rho_w = 1003\ \mathrm{kg\ m^{-3}}$ is the water density and f_w is a friction coefficient. The friction coefficient was determined following Soulsby (1997) as the higher of the rough and smooth bottom estimates:

$$f_w = \max\{f_{wr}, f_{ws}\}, \tag{2}$$

where

$$f_{wr} = 0.237 r^{-0.52}, \tag{3}$$

is the rough bottom friction coefficient, $r = a_{bot}/k_s$, $k_s = 2.5 d_{50}$ is the Nikuradse equivalent sand grain roughness, and

$$f_{ws} = B R_w^{-N} \tag{4}$$

is the smooth bottom friction coefficient. Here $R_w = U_{bot} a_{bot}/\nu$ is the Reynolds number, ν is the kinematic viscosity of water ($1.3 \cdot 10^{-6}$ m^2 s^{-1}, unless given by the in situ measurement), a_{bot} is the amplitude of the wave-induced near-bottom velocities (see Appendix A for a definition), and B and N are constants that depend on the Reynolds number such that:

$$B = 2, N = 0.5 \quad \text{for} \quad R_w \leq 5 \cdot 10^5 (\text{laminar}) \tag{5}$$

$$B = 0.0521, N = 0.187 \quad \text{for} \quad R_w > 5 \cdot 10^5 (\text{turbulent}) \tag{6}$$

2.3.2 Estimated critical stresses, τ_{cr}

The critical value of the shear stress is the value that needs to be exceeded in order for resuspension to take place. The critical value depends on the sea floor properties, and is given by

$$\tau_{cr} = \theta_{cr} (\rho_s - \rho_w) g d_{50} \tag{7}$$

https://doi.org/10.5194/egusphere-2025-2936
Preprint. Discussion started: 3 July 2025

where τ_{cr} ($\mathrm{N\ m^{-2}}$) is the critical shear stress, θ_{cr} is the threshold Shields parameter, g is the gravitational acceleration (9.82 $\mathrm{m\ s^{-2}}$), ρ_s is particle density (2650 $\mathrm{kg\ m^{-3}}$), ρ_w is the water density (1003 $\mathrm{kg\ m^{-3}}$, unless given by in situ measurement) and d_{50} is median grain size (m). The Shields parameter (improved by Soulsby and Whitehouse, 1997) can be estimated as

$$\theta_{cr} = \frac{0.3}{1+1.2D_*} + 0.055\left[1-\exp\left(-0.02D_*\right)\right] \tag{8}$$

where D_* is the dimensionless grain size calculated with

$$D_* = \left(\frac{g(\frac{\rho_s}{\rho_w}-1)}{\nu^2}\right)^{\frac{1}{3}} d_{50}. \tag{9}$$

2.3.3 Experimental critical stresses, $\hat{\tau}_{cr}$

In the 2014 and 2015 field campaigns (Joensuu et al., 2018, 2020), the critical shear stresses from the sediment samples were determined in the laboratory with a portable EROMES device (Schünemann and Kühl, 1991; Andersen, 2001). Bed shear stress on the sediment surface is generated by turbulent fluctuations induced by a propeller and baffle ring. The baffle ring prevents rotational flow and ensures turbulent flow fluctuations mimicking those observed by waves in nature. Suspended solids concentration is monitored with an OBS sensor (optical back-scattering sensor). The propeller revolutions have been calibrated to nominal bed shear stresses (Schünemann and Kühl, 1991; Andersen, 2001).

At each run, the bed shear stress was increased every 2 min by 0.1 $\mathrm{N\ m^{-2}}$ from 0 to 2.0 $\mathrm{N\ m^{-2}}$ in the year 2014 study and from 0 to 1.6 $\mathrm{N\ m^{-2}}$ in the year 2015 study. Water samples for gravimetric analysis were collected during each run to calibrate the OBS sensor into suspended solids concentration (SSC; $\mathrm{mg\ l^{-1}}$) (Andersen, 2001; Andersen and Pejrup, 2002). The critical shear stress ($\mathrm{N\ m^{-2}}$) was defined at the erosion rate of 0.1 ($\mathrm{g\ m^{-2}s^{-1}}$), which describes the erosion after the erosion of unconsolidated "fluffy" material (Andersen, 2001; Andersen et al., 2005). For a more extensive description of the laboratory procedures, see Joensuu et al. (2018, 2020).

3 Results

3.1 Model estimates of shear stresses

The modelled shear stresses were estimated based on the near bottom velocities, and the friction coefficients that were derived from the near bottom wave parameters and the estimated grain sizes. The shear stresses were determined for every model time step from all available data (2014, 2015 and 2017).

Mean modelled stresses were generally below 10 $\mathrm{N\ m^{-2}}$ (Fig. 5a). The 95$^{\mathrm{th}}$ percentiles exceeded 30 $\mathrm{N\ m^{-2}}$ in shallow, exposed areas with large grain sizes (boulders) but remained low (around 5 $\mathrm{N\ m^{-2}}$) near the shoreline (Fig. 5b). Maximum values were concentrated in boulder areas, while the nearshore values stayed below 10 $\mathrm{N\ m^{-2}}$ (Fig. 5c and Fig. 4).

The maximum values indicate that the area around the Tvärminne research station is well sheltered from waves, resulting in very low wave-induced near-bottom shear stresses. The nearest location with notable wave-induced bottom stresses was along the shoreline at longitude 23° 06' – 23° 12', where the bottom type consisted of coarse sediments.

https://doi.org/10.5194/egusphere-2025-2936
Preprint. Discussion started: 3 July 2025

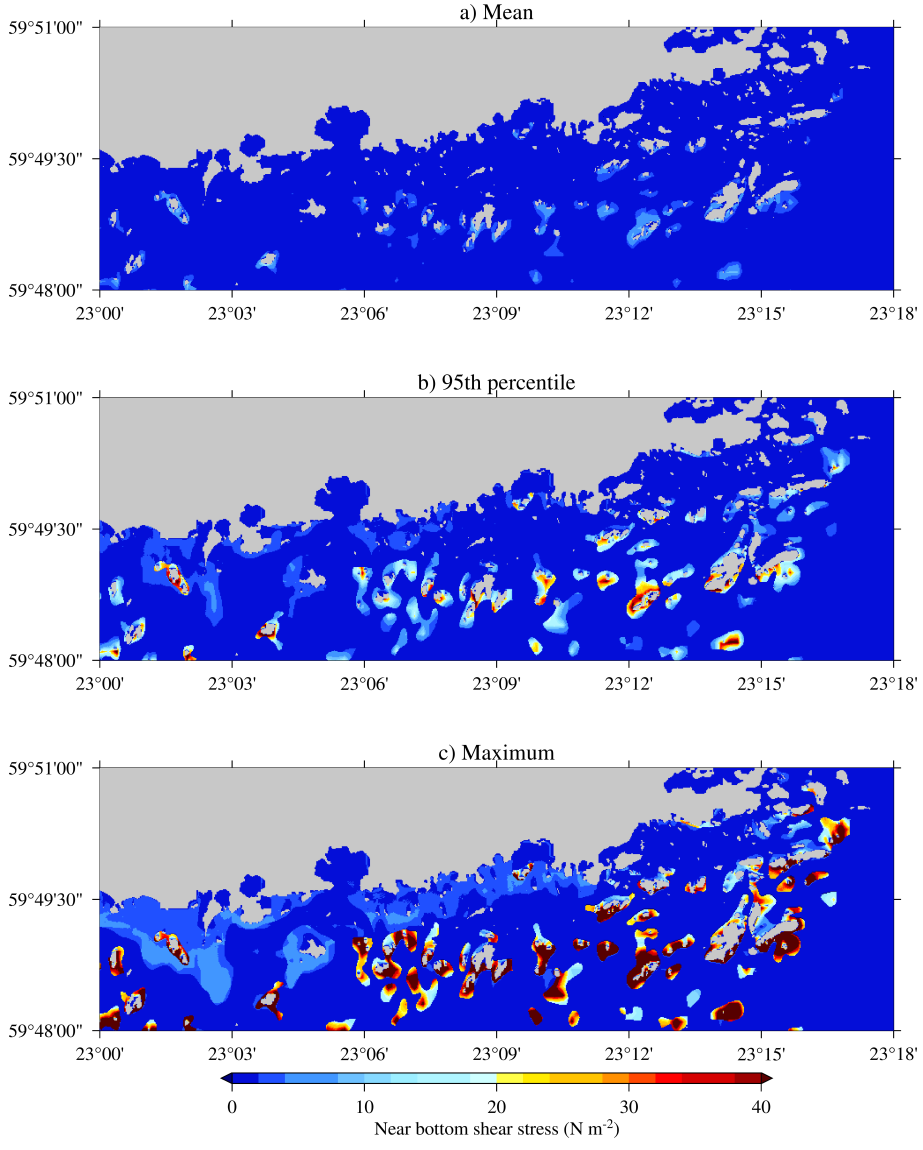

Figure 5. The mean (a), 95^{th} percentile and maximum values of the modelled near bottom shear stress for all the available model data.

3.2 Modelled exceedance of critical values

The modelled near bottom shear stresses were compared to the theoretically derived critical stresses. The exceedance probabilities shown in Fig. 6 indicates the frequency at which wave-induced water motions could theoretically resuspend sediments.

The exceedance probability depends on three main factors: *i)* the wave conditions, *ii)* the water depth, and *iii)* the bottom type. Several sheltered areas are particularly prone to wave-induced resuspension due to shallow depths (which increase shear

https://doi.org/10.5194/egusphere-2025-2936
Preprint. Discussion started: 3 July 2025

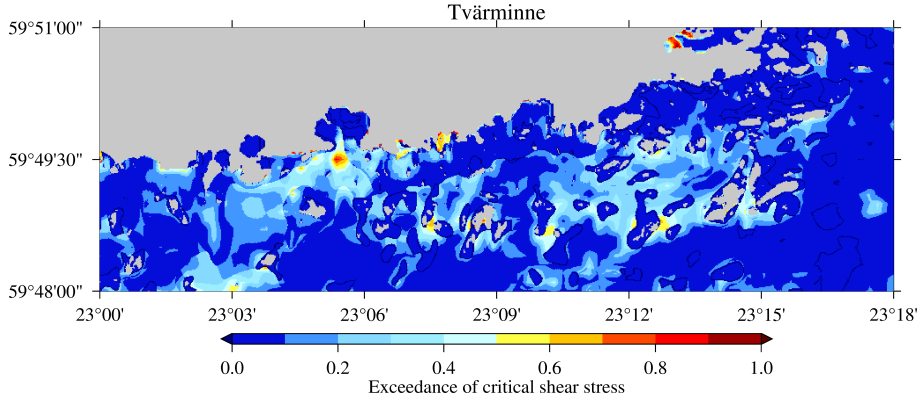

Figure 6. The fraction of times the modelled shear stresses exceeded the modelled critical values.

stress) and fine sediments (which lower the critical stress). There is therefore not a direct connection exceedance probability and the near-bottom velocity maps in Appendix B.

Kahma (2021) estimated the potential for wave-induced near-bottom velocities using the long-wave (7 s) wave heights from a ray-tracing model as a proxy. The results of Kahma (2021) were 10% exceedance values. While they are able to identify some areas that might be vulnerable to higher wave-induced near-bottom velocities, the author noted that they are not a substitute for specifically modelling the near-bottom velocities. The use of wave heights as a proxy can naturally also not account for the variation in the seabed type, as done in this study.

Due to the highly heterogeneous nature of the factors influencing resuspension in the coastal area off Hanko, the resulting exceedance probabilities form a mosaic-like pattern. Notable changes in exceedance values near the shore occur when the bottom type shifts from coarse sediments to sand or mud (Fig. 4), which alters the critical stress, even if wave conditions remain roughly the same. Similar observations were made by Valanko et al. (2010) in the same area, particularly in even shallower regions where waves were the primary driver of resuspension.

Exceedance probabilities were generally under 10%, but larger areas showed a resuspension probability ranging from 20 and 50 %. These areas were not limited to the coast but also appeared within a group of islands and islets located about 2–3 km from the shoreline, where the water is shallow. Exceedance probabilities above 50% were found only in small, isolated regions, and the probability of exceeding 70% was restricted to areas close to the coast.

3.3 Wave-induced stresses during representative high-wind events

We now present the modelled near bottom shear stresses during high winds blowing from the southerly sector between SW and SSE in late November 2015, when sustained wind speeds exceeding 20 m s^{-1} and gusts approaching 26 m s^{-1} were recorded at the FMI Hanko Russarö automatic weather station (59°46'25.08" N 22°56'55.26" E), 18 km SW from the Tvärminne station. These episodes offer valuable insight into how strong winds trigger wave-induced sediment resuspension in the area.

https://doi.org/10.5194/egusphere-2025-2936
Preprint. Discussion started: 3 July 2025

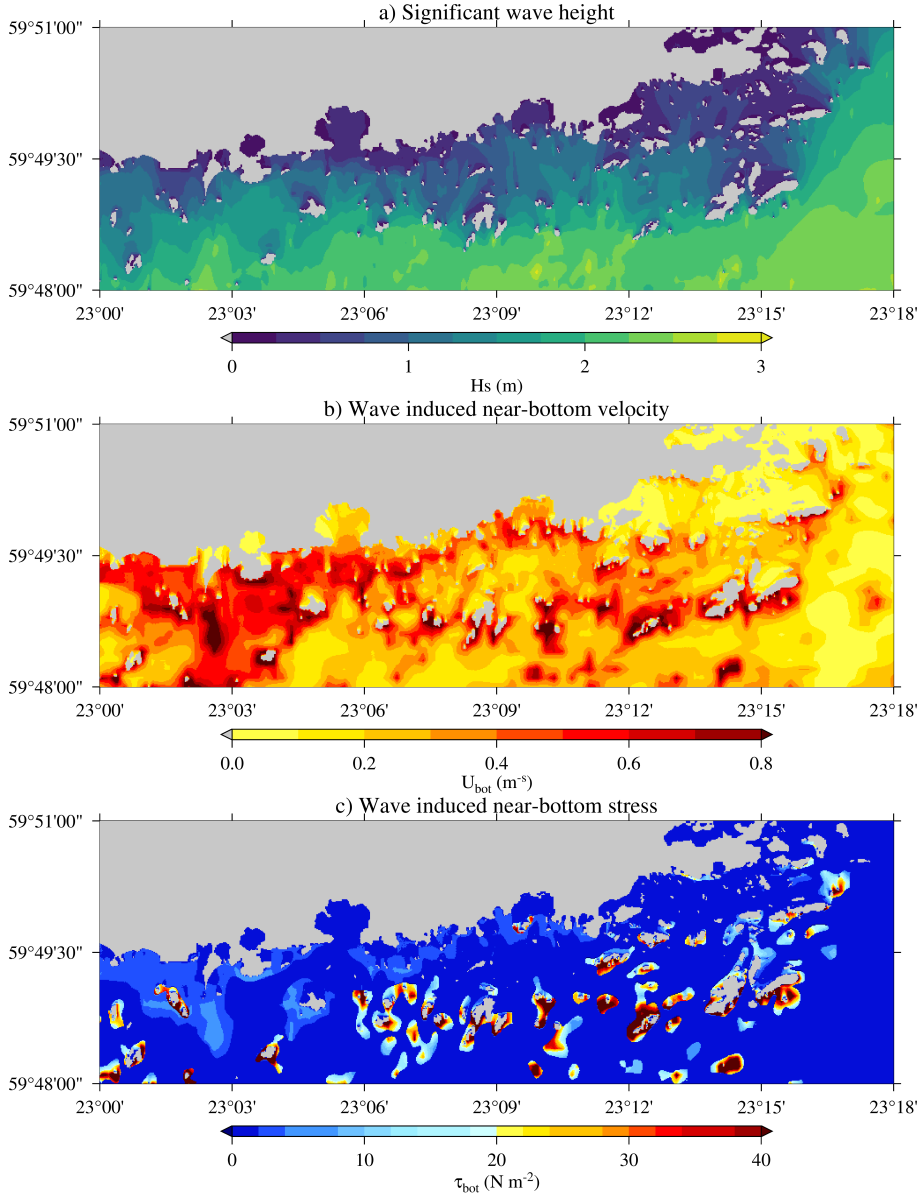

Figure 7. The significant wave height (a), near-bottom orbital velocities (b) and stresses (c) for 28 November 2015 22 UTC.

On 27 and 28 November, southwesterly (200–243°) winds of approximately 19–20 m s^{-1} gradually shifted to a more southerly direction (165–171°) by 29 November. Southwesterly winds are common in this region and can generate large waves that propagate into nearshore areas. On 28 November the significant wave height outside the edge of the archipelago was close to 3 m, still being around 2 m inside the archipelago (Fig. 7a). The wave height was reduced significantly near the shore, but since the wave-induced near-bottom orbital velocities are also determined by the wave period, they were still in the order of

https://doi.org/10.5194/egusphere-2025-2936
Preprint. Discussion started: 3 July 2025

0.5 $\mathrm{m\ s^{-1}}$ for large stretches of the coastline (Fig. 7b). The wave-induced shear stress near the bottom was modelled to exceed 2 $\mathrm{N\ m^{-2}}$ at some points near the coast (Fig. 7c), which is around the limit for the modelled critical shear stress for coarse sediments (Table 1). The highest values were modelled where the bottom type was Boulders, since the modelled stress depends on the grain size through Eq. 3.

The most intense storm in 2015 occurred on the morning of 30 November, when sustained wind speeds of 23–25 $\mathrm{m\ s^{-1}}$ were recorded from roughly 150–160° (SSE). A peak wind of 26.2 $\mathrm{m\ s^{-1}}$ was measured at 11:00 local time. Winds from this direction generated waves exceeding 4 m that propagated through the outer archipelago, funneling energy into shallower inshore areas (Fig. 8a). The wave model suggest that in some shallow locations, near-bottom orbital velocities can be close to 1 $\mathrm{m\ s^{-1}}$ in particularly exposed coastal locations (Fig. 8b).

The modelled near-bottom shear stress near the coast exceeded 2 $\mathrm{N\ m^{-2}}$ (Fig. 8c). Such elevated stresses are capable of resuspending not only fine sediments but also coarser fractions, potentially leading to abrupt increases in turbidity and nutrient fluxes.

While local bathymetry and island shielding moderate the spatial extent of wave action, shallow areas exposed to the prevailing wind direction remain particularly vulnerable. These observations align with the numerical model findings, which indicate that frequent resuspension events can occur even in sheltered archipelago regions. However, actual resuspension thresholds depend strongly on sediment composition, biological stabilization (e.g., biofilms, vegetation), and temporal variations in bulk density – factors that can render real-world resuspension patterns more complex than those predicted by simple grain-size models.

Overall, the November 2015 wind events provide a clear example of how episodic storms can rapidly mobilize coastal sediments in the Baltic Sea's archipelago, with significant implications for water quality and benthic ecosystems.

3.4 Comparison to measured critical stresses

Even though the modelled critical stresses are based on the best available data on wave conditions and bottom type, they do not account for the variability in actual grain sizes, their potential mixed distributions, or other factors, such as biological activity, that could influence resuspension events.

To assess this uncertainty in the model data, we compared the theoretical critical stresses to experimental values obtained in the laboratory from in situ samples. The experimental critical shear stresses, measured with the EROMES device, were notably higher ($\hat{\tau}_{cr}$ = 0.45–1.56 $\mathrm{N\ m^{-2}}$) compared to the theoretical critical shear stresses derived from modelled grain sizes ($\tau_{cr}(d_{50})$= 0.13–0.21 $\mathrm{N\ m^{-2}}$) or from measured grain sizes ($\tau_{cr}(\hat{d}_{50})$=0.11–0.28 $\mathrm{N\ m^{-2}}$) (see Table 2).

These discrepancies indicate that while the modelled critical shear stresses are routinely exceeded, the modelled shear stresses rarely surpass the critical stress values determined by the EROMES device from in situ samples. In fact, at most locations, the measured critical stress is never exceeded. The exception is location ID11, where the modelled shear stresses exceed the measured value of 1.13 $\mathrm{N\ m^{-2}}$ (Fig. 9). While the depth and bottom type is similar at both ID06 and ID11, ID06 is clearly more sheltered during strong wave events, as seen in Fig. 7 and 8. More generally, we also modelled shear stresses exceeding 2 $\mathrm{N\ m^{-2}}$ in larger areas near the coast during the SSE winds on 30 November 2015 (Fig. 8), which exceeds the

https://doi.org/10.5194/egusphere-2025-2936
Preprint. Discussion started: 3 July 2025

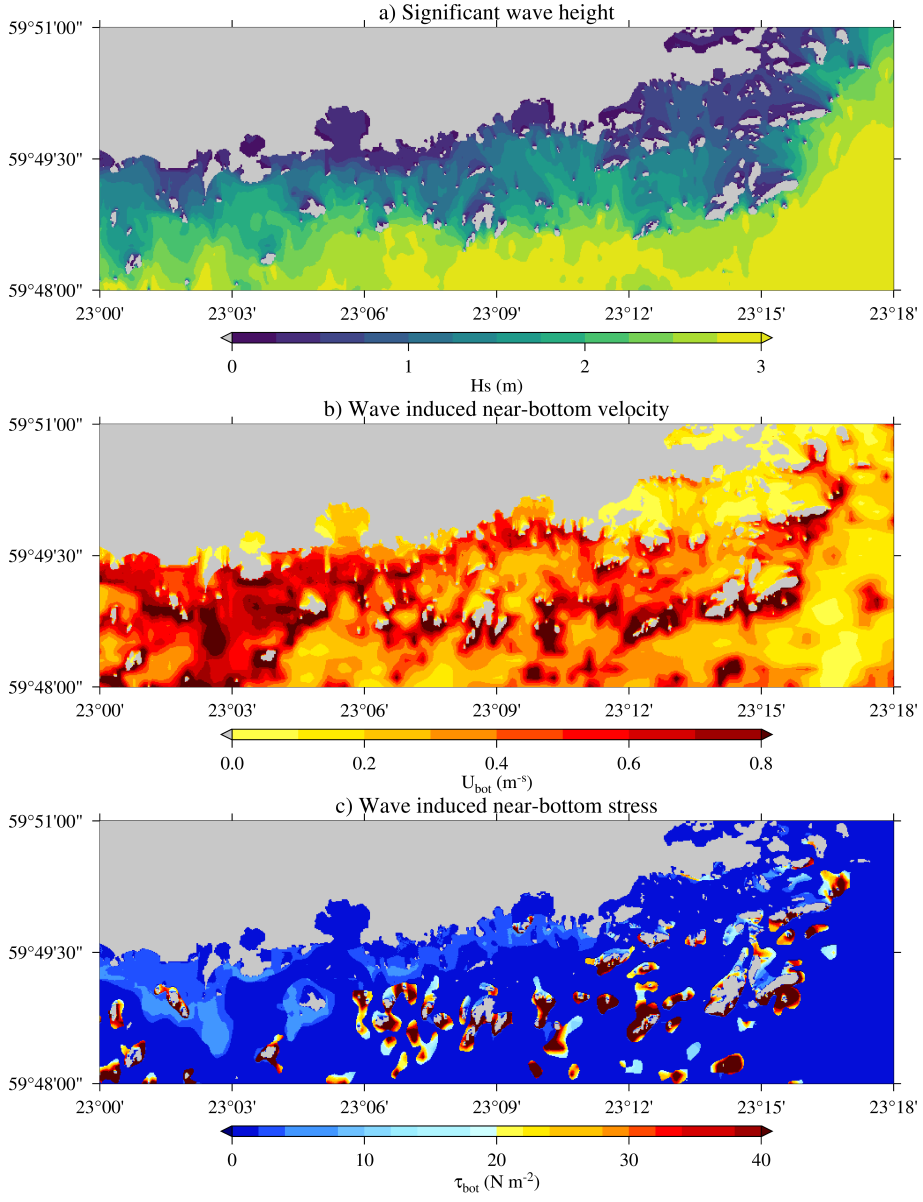

Figure 8. The significant wave height (a), near-bottom orbital velocities (b) and stresses (c) for 30 November 2015 10 UTC.

theoretical critical shear stress for coarser sediments (Table 1) and the measured critical shear stresses at all measurement locations.

The modelled critical stresses – which are based solely on the median grain size – lack biogeochemical factors such as sediment particle size distribution and bulk density, which are central in explaining the critical shear stresses observed in in situ sediment samples (Grabowski et al., 2011; Jepsen et al., 1997).

https://doi.org/10.5194/egusphere-2025-2936
Preprint. Discussion started: 3 July 2025

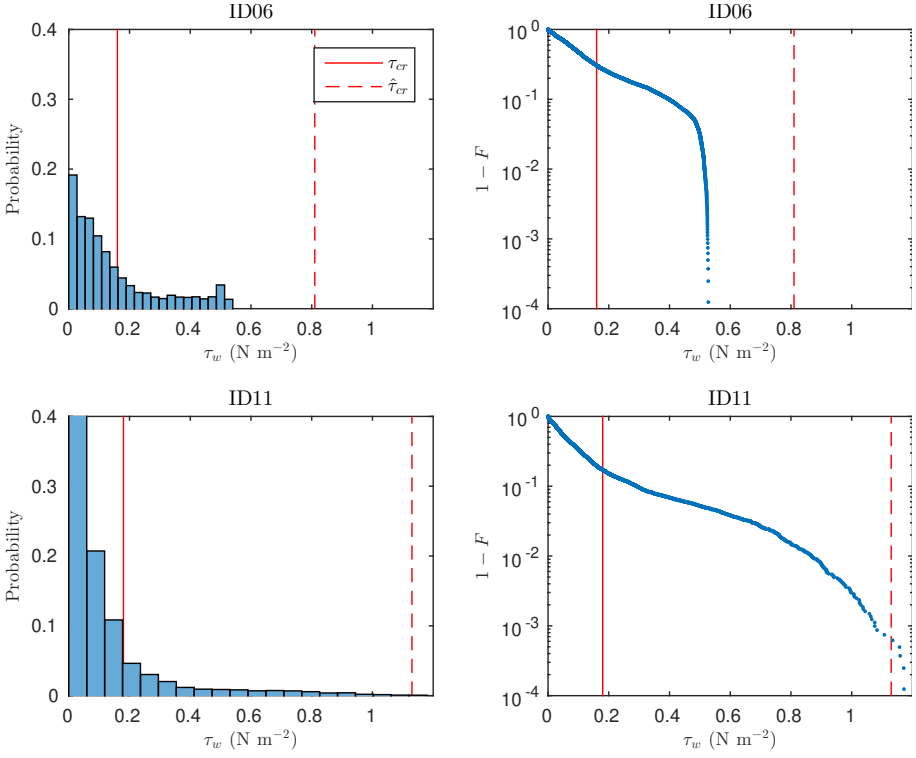

Figure 9. Distributions of modelled shear stresses at two of the most exposed locations. Here, F represents the cumulative distribution function, with the y-axis on the right indicating the probability of exceedance. The solid and dashed lines correspond to the modelled and measured critical shear stress values, respectively.

4 Discussion

The erodibility of natural sediments is influenced by variations in their physical, geochemical, and biological properties. For example, benthic fauna can modify sediment erodibility by altering water content, bulk density, and the particle size distribution through bioturbation activities (de Deckere et al., 2001; Le Hir et al., 2007). The experimental critical shear stresses used in this study were derived from natural submerged sediment samples, which account for the naturally occurring variability over both time (Joensuu et al., 2020) and space (Joensuu et al., 2018). Nonetheless, the theoretical (modelled) shear stresses were lower than the experimental values by factors ranging from 3.9–8.4 for mixed sediments, 3.3–4.7 for mud, and 2.7–8.2 for sand.

Several potential errors could explain the large discrepancies between observed and modelled critical shear stresses. First, the wave model itself might be inaccurate. The water depth used in the wave model directly influences the results, as surface waves are affected by factors like bottom friction and wave breaking, both of which depend on local water depth. More critically, the water depth is essential for transferring surface wave energy to the bottom, as wave motion attenuates rapidly with depth. This sensitivity is evident from wave measurements made with the inner wave buoy, where the water depth is approximately 17 metres; if a 15 meter depth is used to transfer the measured surface waves to the seafloor, the mean orbital velocities

https://doi.org/10.5194/egusphere-2025-2936
Preprint. Discussion started: 3 July 2025

Table 2. The depth (m), median grain size, d_{50} (mm), the modelled 95^{th} percentile and maximum stress, τ_w (N m^{-2}), and the critical shear stresses, τ_{cr} (N m^{-2}), at each measurement location (see Fig. 2). Measured values are denoted by a hat (e.g. $\hat{d}_{50}$). The theoretical critical shear stress has been determined using both the modelled grain size, $\tau_{cr}(d_{50})$, and the measured grain size, $\tau_{cr}(\hat{d}_{50})$.

Site	Depth	Type (in situ)	d_{50}	$\hat{d}_{50}$	τ_w^{95th}	$\tau_w^{\max}$	$\tau_{cr}(d_{50})$	$\tau_{cr}(\hat{d}_{50})$	$\hat{\tau}_{cr}$
ID01	3.9	Mixed sediment	0.15	0.16	0.03	0.10	0.14	0.14	0.78
ID02	3.2	Sand	0.34	0.29	0.04	0.29	0.19	0.18	1.16
ID03	3.0	Mixed sediment	0.15	0.13	0.03	0.17	0.14	0.13	1.12
ID04	2.3	Mud	0.09	0.06	0.01	0.05	0.13	0.11	0.54
ID05	2.6	Sand	0.34	0.33	0.04	0.09	0.19	0.19	0.62
ID06	3.0	Sand	0.34	0.22	0.50	0.54	0.20	0.16	0.81
ID07	3.0	Sand	0.34	0.57	0.05	0.15	0.20	0.28	0.76
ID09	3.0	Mixed sediment	0.15	0.17	0.08	0.19	0.16	0.16	0.95
ID10	3.8	Sand	0.34	0.44	0.17	0.19	0.20	0.23	0.94
ID11	3.2	Sand	0.34	0.26	0.53	1.21	0.20	0.18	1.13
ID14	3.4	Sand	0.34	0.27	0.05	0.14	0.21	0.19	1.56
ID15	3.7	Mixed sediment	0.15	0.15	0.02	0.06	0.15	0.15	0.59
ID16	3.5	Mud	0.09	0.12	0.02	0.06	0.13	0.14	0.45

increase by 26% (not shown). While inaccuracies in water depth of this magnitude are possible, they are insufficient to account for the observed discrepancies (200–700%), and the sensitivity should decrease in extremely shallow depths, as horizontal wave motion does not attenuate significantly when the wavelength is at least 20 times the water depth. Furthermore, accurate estimates of near-bottom mean currents were not available for this study, and the absence of current data likely biases the resuspension probabilities toward lower values. Nevertheless, current speeds are expected to be relatively low compared to the maximum wave-induced velocities, especially since tidal currents in the the Balitic Sea are generally weak.

A second potential source of error is the spatial grain size data. These data were only available in broad categories (e.g., sand, coarse sediments), leading to significant uncertainty regarding the actual median grain size at specific locations, particularly for mixed sediments. However, using the measured median grain size in the theoretical calculations (column $\tau_{cr}(\hat{d}_{50})$ in Table 2) did not significantly alter the results at the sample locations. It is important to note, though, that this agreement does not validate the accuracy of the modelled median grain sizes in other areas.

The third source of discrepancy stems from the reliance on the median grain size alone to model erodability, although e.g. large variations in the grain size distribution might cause armoring effects. There is no consensus on the correct form of the wave friction factor, and our results suggest this was the primary cause of error in our study. This presents a two-fold challenge for modelling sediment resuspension: *i)* how can this effect be parameterized in a practical yet accurate way, and *ii)* is it possible to acquire the necessary data for such parameterization?

https://doi.org/10.5194/egusphere-2025-2936
Preprint. Discussion started: 3 July 2025

In addition to the actual grain size distribution, it is well known that biota plays a significant role in the erodability of sediments, both directly and indirectly. Directly, it affects bed roughness and structure, while indirectly, it influences bulk density, porosity, and particle size distribution. Bulk density is the mass of sediment per unit volume, including the pore spaces, and it is negatively correlated with erodibility. Sediments with high bulk density are more compacted, making them more resistant to hydrodynamic forcing and requiring higher shear stIDress to initiate erosion. In contrast, low bulk density sediments are typically loose, unconsolidated, and often freshly deposited. These sediments contain more water and pore space, making them structurally weaker and more susceptible to erosion under relatively low hydrodynamic energy. Although erodability could be described using bulk density – whether or not biota is present – we also know that biological activity varies over time. These temporal fluctuations, such as seasonal changes, induce variations in properties like bulk density, complicating the mapping of seafloor characteristics.

Our results indicate that sediment resuspension potential in the study area is highly heterogeneous, even without considering biological factors. These challenges raise questions about the practical applicability of a more complex erodability model, even if an accurate one were available. One possible approach could involve a modified median grain size model, which, while non-physical, could implicitly account for other variations (e.g., bulk density) by increasing the grain size. However, this model would no longer accurately represent the actual grain sizes at the seafloor and would need to be calibrated separately for each area.

Despite the inherent uncertainties in the forcing data, the modelled near-bottom shear stresses suggest that wind-driven waves can initiate frequent sediment resuspension events, even in more sheltered areas of the archipelago. High-wind events, in particular, may cause significant resuspension, impacting water quality and nutrient cycling. It is likely that the modelled resuspension frequencies are overestimated, with accuracy depending on local sedimentary environments, habitat structure, and benthic biota. Until further studies reduce the uncertainties in modelled critical shear stresses, the exceedance probability maps should be interpreted more qualitatively than quantitatively.

5 Conclusions

This study implemented a numerical spectral wave model (SWAN) with an exceptionally high spatial resolution (20 m) for the coastal archipelago area of Hanko in the Baltic Sea. The near-bottom wave parameters from the wave model were combined with median grain sizes (d_{50}) estimated from available spatial data of the seabed type. We also calculated d_{50}-based critical shear stresses and compared them with laboratory values previously determined from in situ samples collected in the area. Finally, we estimated exceedance frequencies based on the hourly model data.

The high-resolution wave data revealed that wave-induced near-bottom velocities are highly variable in the complex coastal archipelago of the study area. When combined with the rapidly changing depth and seabed conditions, the modelled shear stresses and sediment resuspension probabilities exhibited extreme heterogeneity.

The critical shear stresses derived from in situ samples were 3–8 times higher than the theoretical values calculated using d_{50} grain size estimates. These differences were large enough to reduce the resuspension probability from approximately $\sim$15 % to

https://doi.org/10.5194/egusphere-2025-2936
Preprint. Discussion started: 3 July 2025

near 0 % at some of the sample stations. The proposed explanation for these significant discrepancies lies in the biogeochemical properties of the sediments.

In conclusion, the highly heterogeneous conditions limit the ability to map sediment resuspension potential in complex coastal areas using only in situ samples. The numerical wave model can accurately simulate the highly variable wave conditions, making it useful for studies on carbon cycling or the likelihood of organic matter resuspension. However, our findings suggest that even with highly accurate wave, depth, and seabed data, reliable estimates of sediment resuspension probabilities cannot be achieved without considering the biological and biogeochemical properties when estimating critical shear stresses.

Code and data availability. The seabed data can be accessed through https://www.emodnet-geology.eu/data-products/seabed-substrates/. The open source SWAN model can be downloaded at https://swanmodel.sourceforge.io/. The wave buoy data is archived in a repository (Björkqvist et al., 2025) and will be opened upon the acceptance of the manuscript. The sediment data from 2014 and 2015 are archived in a repository (Savela, 2025) and will be opened upon the acceptance of the manuscript.

Appendix A: Definition of wave parameters

Third generation numerical wave models model the so called wave spectrum $S(\omega)$ $(\mathrm{m^2 s})$, which gives the variance density of waves of different (angular) frequency $\omega = 2\pi f$ $(\mathrm{rad\ s^{-1}})$ and direction, θ (rad), where f (Hz) is the linear frequency. The variance of a wave component is directly proportional to the square of its height, which is directly proportional to its energy.

The wave model solves the action balance equation, not the energy balance equation, since the spectral variance density is only conserved in deep water without currents. Since this study did not use currents, we give the action balance equation below without currents:

$$\frac{\partial N}{\partial t} + \nabla_{\boldsymbol{x}} \cdot (\boldsymbol{c}_g N) + \frac{\partial c_\sigma N}{\partial \sigma} + \frac{\partial c_\theta N}{\partial \theta} = \frac{G_{tot}}{\sigma}, \tag{A1}$$

where $N = S/\sigma$ is the wave action, c_g is the group speed of a wave component, c_σ and c_θ signifies the speed of the change in frequency and direction, $\nabla_{\boldsymbol{x}}$ is the spatial partial derivative, and G_{tot} is a sum of the so called source terms, which model the different physical processes that add, remove or redistribute energy of the wave components. Without currents the intrinsic frequency σ $(\mathrm{rad\ s^{-1}})$ equals the angular frequency ω.

The wave parameters were calculated from the modelled or measured wave spectrum. First, the near-bottom wave spectrum was calculated:

$$S_b(\omega) = \frac{S(\omega)}{\sinh^2 kh}, \tag{A2}$$

where $S(\omega)$ $(\mathrm{m^2 s})$ is the aforementioned surface wave spectrum, h (m) is the water depth, and k $(\mathrm{rad\ m^{-1}})$ is the wavenumber solved from wave frequency using linear wave theory. Note, that the wave spectrum from both wave measurements and

https://doi.org/10.5194/egusphere-2025-2936
Preprint. Discussion started: 3 July 2025

model output is usually given as a function of f, and in this case $E(f) = 2\pi S(\omega)$ ($\mathrm{m^2 Hz^{-1}}$) to conserve the area under the spectral curve (i.e. the total variance of the wave field).

The maximum near bottom orbital velocity U_{bot} ($\mathrm{m\ s^{-1}}$) is defined using the near bottom spectrum as

$$U_{bot} = \sqrt{2 \int S_b(\omega) \omega^2 \, \mathrm{d}\omega} = \sqrt{2} U_{rms}, \tag{A3}$$

where U_{rms} is the root-mean-square orbital velocity at the bottom.

The near bottom amplitude a_{bot} (m) is defined as

$$a_{bot} = \sqrt{2 \int S_b(\omega) \, \mathrm{d}\omega}, \tag{A4}$$

while the near bottom mean wave period is defined as

$$T_{m_{bot}} = 2\pi \sqrt{\frac{\int S_b(\omega) \, \mathrm{d}\omega}{\int S_b(\omega) \omega^2 \, \mathrm{d}\omega}} = \sqrt{\frac{\int E_b(f) \, \mathrm{d}f}{\int E_b(f) f^2 \, \mathrm{d}f}}. \tag{A5}$$

The relationship between these three parameters is therefore

$$a_{bot} = \frac{T_{m_{bot}} U_{bot}}{2\pi}, \tag{A6}$$

meaning that two of them exactly determines the third.

Appendix B: Near-bottom velocities, U_{bot}

Figure A1 shows the mean, 95^{th} percentile and max values of the modelled near bottom velocities. These velocities are based purely on the wave model data, and don't contain any effects from the chosen grain sizes.

Author contributions. The study was initiated by MS and AN, and further conceptualized by MS, AN, HP and JVB. Majority of the sediment samples were collected by AN and analyzed by MS. The critical shear stresses from the samples were determined by MS. The wave model simulations were performed by VA and processed by JVB. The theoretical shear stresses were determined by HP and JVB. The wave measurements were processed by JVB. The manuscript was prepared by JVB and MS with contributions from all authors.

Competing interests. The authors declare that they have no competing interests.

https://doi.org/10.5194/egusphere-2025-2936
Preprint. Discussion started: 3 July 2025

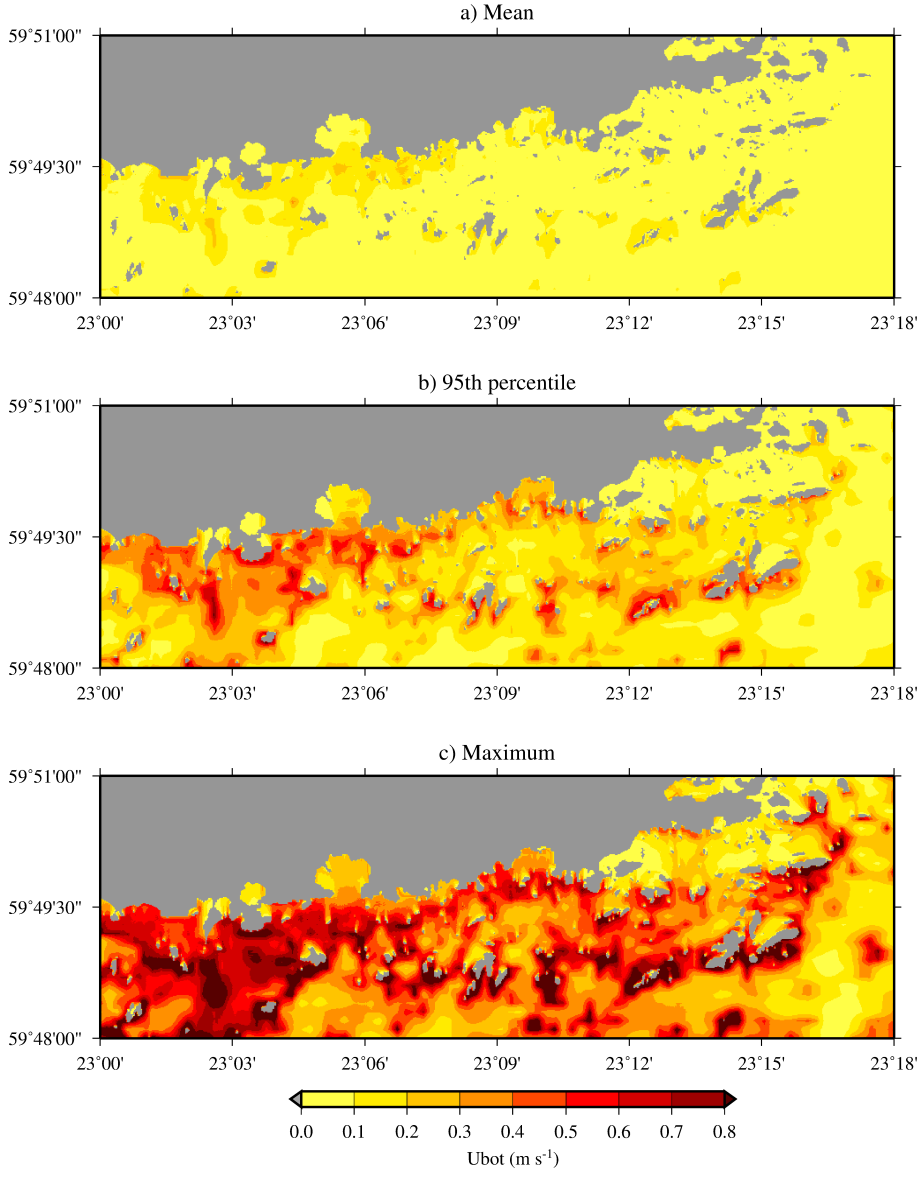

Figure A1. Near bottom velocities (U_{bot}) as modelled by the SWAN model.

Acknowledgements. Data used in this publication was made available by the EMODnet Geology project, http://www.emodnet-geology.eu funded by the European Commission Directorate General for Maritime Affairs and Fisheries. These data were collected by the Geological Survey of Finland. We thankfully acknowledge the work by the FMI technical staff in deploying and retrieving the wave buoys. This project got funding from Walter and Andrée de Nottbeck Foundation and Onni Talas Foundation (MS).

https://doi.org/10.5194/egusphere-2025-2936
Preprint. Discussion started: 3 July 2025

References

Abdolali, A., Roland, A., van der Westhuysen, A., Meixner, J., Chawla, A., Hesser, T. J., Smith, J. M., and Sikiric, M. D.: Large-scale hurricane modeling using domain decomposition parallelization and implicit scheme implemented in WAVEWATCH III wave model, Coastal Engineering, 157, 103 656, https://doi.org/https://doi.org/10.1016/j.coastaleng.2020.103656, 2020.

Alari, V. and Raudsepp, U.: Simulation of Wave Damping Near Coast due to Offshore Wind Farms, Journal of Coastal Research, 28, 143 – 148, https://doi.org/10.2112/JCOASTRES-D-10-00054.1, 2012.

Alenius, P., Myrberg, K., and Nekrasov, A.: The physical oceanography of the Gulf of Finland: a review, Boreal Environ. Res, 3, 97–125, 1998.

Andersen, T.: Seasonal variation in erodibility of two temperate, microtidal mudflats, Estuarine, Coastal and Shelf Science, 53, 1–12, 2001.

Andersen, T. J. and Pejrup, M.: Biological Mediation of the Settling Velocity of Bed Material Eroded from an Intertidal Mudflat, the Danish Wadden Sea, Estuarine, Coastal and Shelf Science, 54, 737–745, https://doi.org/https://doi.org/10.1006/ecss.2001.0856, 2002.

Andersen, T. J., Lund-Hansen, L. C., Pejrup, M., Jensen, K. T., and Mouritsen, K. N.: Biologically induced differences in erodibility and aggregation of subtidal and intertidal sediments: a possible cause for seasonal changes in sediment deposition, Journal of Marine Systems, 55, 123–138, https://doi.org/https://doi.org/10.1016/j.jmarsys.2004.09.004, 2005.

Björkqvist, J.-V., Pettersson, H., and Roine, T.: Wave buoy data from the Tvärminne area from 2017, https://doi.org/10.5281/zenodo.15781282, 2025.

Black, K. S., Tolhurst, T. J., Paterson, D. M., and Hagerthey, S. E.: Working with Natural Cohesive Sediments, Journal of Hydraulic Engineering, 128, 2–8, https://doi.org/10.1061/(ASCE)0733-9429(2002)128:1(2), 2002.

Booij, N., Ris, R., and Holthuijsen, L. H.: A third-generation wave model for coastal regions 1. Model description and validation, Journal of Geophysical Research, 104, 7649–7666, https://doi.org/10.1029/98jc02622, 1999.

Dade, W., Nowell, A., and Jumars, P.: Predicting erosion resistance of muds, Marine Geology, 105, 285–297, https://doi.org/https://doi.org/10.1016/0025-3227(92)90194-M, 1992.

Datawell, B.: Datawell Waverider Reference Manual, Tech. rep., http://www.datawell.nl/Support/Documentation/Manuals.aspx, 2017.

de Deckere, E., Tolhurst, T., and de Brouwer, J.: Destabilization of Cohesive Intertidal Sediments by Infauna, Estuarine, Coastal and Shelf Science, 53, 665–669, https://doi.org/https://doi.org/10.1006/ecss.2001.0811, 2001.

Decho, A. W.: Microbial biofilms in intertidal systems: an overview, Continental Shelf Research, 20, 1257–1273, https://doi.org/https://doi.org/10.1016/S0278-4343(00)00022-4, 2000.

Eerola, K.: Twenty-One Years of Verification from the HIRLAM NWP System, Weather and Forecasting, 28, 270 – 285, https://doi.org/https://doi.org/10.1175/WAF-D-12-00068.1, 2013.

Grabowski, R. C., Droppo, I. G., and Wharton, G.: Erodibility of cohesive sediment: The importance of sediment properties, Earth-Science Reviews, 105, 101–120, 2011.

Harris, R. J., Pilditch, C. A., Hewitt, J. E., Lohrer, A. M., Van Colen, C., Townsend, M., and Thrush, S. F.: Biotic interactions influence sediment erodibility on wave-exposed sandflats, Marine ecology progress series, 523, 15–30, 2015.

Jepsen, R., Roberts, J., and Lick, W.: Effects of Bulk Density on Sediment Erosion Rates, Water, Air, and Soil Pollution, 99, 21–31, https://doi.org/10.1023/A:1018355626070, 1997.

https://doi.org/10.5194/egusphere-2025-2936
Preprint. Discussion started: 3 July 2025

Joensuu, M., Pilditch, C. A., Harris, R., Hietanen, S., Pettersson, H., and Norkko, A.: Sediment properties, biota, and local habitat structure explain variation in the erodibility of coastal sediments, Limnology and Oceanography, 63, 173–186, https://doi.org/https://doi.org/10.1002/lno.10622, 2018.

Joensuu, M., Pilditch, C. A., and Norkko, A.: Temporal Variation in Resuspension Potential and Associated Nutrient Dynamics in Shallow Coastal Environments, Estuaries and Coasts, 43, 1361–1376, https://doi.org/10.1007/s12237-020-00726-z, 2020.

Kahma, K. K.: Wind-generated long wave climate in the Tvärminne area, Geophysica, 56, 29–37, 2021.

Kaskela, A. M., Kotilainen, A. T., Alanen, U., Cooper, R., Green, S., Guinan, J., van Heteren, S., Kihlman, S., Van Lancker, V., Stevenson, A., and the EMODnet Geology Partners: Picking Up the Pieces—Harmonising and Collating Seabed Substrate Data for European Maritime Areas, Geosciences, 9, https://doi.org/10.3390/geosciences9020084, 2019.

Koch, E. W., Ackerman, J. D., Verduin, J., and Keulen, M. v.: Fluid Dynamics in Seagrass Ecology—from Molecules to Ecosystems, pp. 193–225, Springer Netherlands, Dordrecht, https://doi.org/10.1007/978-1-4020-2983-7_8, 2006.

Komar, P. and Miller, M.: The Threshold of Sediment Movement Under Oscillatory Water Waves, J. sedim. Petrol., 43, https://doi.org/10.1306/74D7290A-2B21-11D7-8648000102C1865D, 1973.

Le Hir, P., Monbet, Y., and Orvain, F.: Sediment erodability in sediment transport modelling: Can we account for biota effects?, Continental Shelf Research, 27, 1116–1142, https://doi.org/https://doi.org/10.1016/j.csr.2005.11.016, 2007.

Madsen, J., Chambers, P., James, W., Koch, E., and Westlake, D.: The interaction between water movement, sediment dynamics and submersed macrophytes, Hydrobiologia, 444, 71–84, https://doi.org/10.1023/A:1017520800568, 2001.

Michaud, E., Desrosiers, G., Mermillod-Blondin, F., Sundby, B., and Stora, G.: The functional group approach to bioturbation: II. The effects of the Macoma balthica community on fluxes of nutrients and dissolved organic carbon across the sediment–water interface, Journal of Experimental Marine Biology and Ecology, 337, 178–189, 2006.

Miettunen, E.: Circulation and transport dynamics in the Archipelago Sea, http://hdl.handle.net/10138/587710, 2024.

Mulsow, S., Boudreau, B. P., and Smith, J. A.: Bioturbation and porosity gradients, Limnology and Oceanography, 43, 1–9, 1998.

Pettersson, H., Kahma, K. K., and Tuomi, L.: Wave Directions in a Narrow Bay, Journal of Physical Oceanography, 40, 155–169, https://doi.org/10.1175/2009JPO4220.1, 2010.

Roberts, J., Jepsen, R., Gotthard, D., and Lick, W.: Effects of Particle Size and Bulk Density on Erosion of Quartz Particles, Journal of Hydraulic Engineering, 124, 1261–1267, https://doi.org/10.1061/(ASCE)0733-9429(1998)124:12(1261), 1998.

Savela, M.: Hydrological and sediment dataset from the Tvärminne coastal area (2014-2015), https://doi.org/https://doi.org/10.5281/zenodo.15796802, 2025.

Schünemann, M. and Kühl, H.: A device for erosion-measurements on naturally formed, muddy sediments: the EROMES-System, GKSS-Forschungszentrum, 1991.

Shields, A.: Application of similarity principles and turbulence research to bed-load movement, 1936.

Soulsby, R.: Dynamics of marine sands, Thomas Telford Publishing, London, UK, 1997.

Soulsby, R. L. and Whitehouse, R. J. S.: Threshold of Sediment Motion in Coastal Environments, https://search.informit.org/doi/10.3316/informit.929741720399033, 1997.

Valanko, S.: Dispersal and metacommunity dynamics in a soft-sediment benthic system: how well is the seafloor connected?, 2012.

Valanko, S., Norkko, A., and Norkko, J.: Strategies of post-larval dispersal in non-tidal soft-sediment communities, Journal of Experimental Marine Biology and Ecology, 384, 51–60, https://doi.org/https://doi.org/10.1016/j.jembe.2009.12.012, 2010.

https://doi.org/10.5194/egusphere-2025-2936
Preprint. Discussion started: 3 July 2025

Westerlund, A., Tuomi, L., Alenius, P., Miettunen, E., and Vankevich, R. E.: Attributing mean circulation patterns to physical phenomena in the Gulf of Finland, Oceanologia, 60, 16–31, https://doi.org/https://doi.org/10.1016/j.oceano.2017.05.003, 2018.